B, N, S heteroatom-doped laser-induced porous PES-derived graphene for high performance supercapacitor

Hanqing Gao[1], Longkun Yang[1], Xiangyu Han, Ziqi Peng, Xinzhi Sun*

College of Chemistry and Pharmaceutical Sciences, Qingdao Agricultural University, ChangCheng Road 700, Chengyang, Qingdao 266109, People's Republic of China

*Corresponding author

E-mail: xzsun@qau.edu.cn

Material and methods

Experimental materials

Chemical reagent materials, such as dimethylformamide, urea, boric acid, ethanol, KOH (analytical grade, solid content 90%) were purchased from Macklin (Shanghai, China), which were not purified further.

Preparation of N, B co-doped S-laser-induced graphene composites

Synthesis of nitrogen and boron co-doped S-laser-induced graphene were prepared with the following process.

0.025 g of boric acid was dissolved in 10 mL of dimethylformamide (DMF), and 1.5 g of polyethersulfone (PES, containing sulfur by itself) powder was added to the boric acid solution, resulting in a uniform viscous solution after stirring sharply. The viscous homogeneous solution was left to stand for 1 h. Last, 5.0 mL of the solution was cast into a mold and dried overnight in an oven, which the dried white films were obtained, marked as B-PES film.

B-PES films were irradiated under CO_2 laser (10.6 μm, Epilog Laser MINI, 40 W) and boron-doped laser-induced graphene was prepared, denoted as BS-LIG. Repeating the first step of preparing a viscous homogenous solution, boric acid is replaced with 0.05g urea, and BS-LIG is incorporated into the viscous solution. The dried film is denoted as BS-LIG-NPES. Under the same laser engraving conditions, the secondary engraved graphene is obtained, denoted as NBS-LIG. Throughout the whole process, the laser scanning speed and resolution were set at 16.6 mm s^{-1} and 1200 dpi, respectively, with laser powers selected at 4 W and 6 W. It is particularly noteworthy that the parameters for both laser irradiations were identical.

As the addition sequence of boric acid and urea is reversed, the final product is BNS-LIG. And boric acid and urea are doped simultaneously; the final product is (NB)S-LIG.

If the laser power is 6 W, the samples are labelled as NBS-LIG, BNS-LIG and (NB)S-LIG. As the laser power is 4 W, the samples are marked as NBS-LIG-4W, BNS-LIG-4W and (NB)S-LIG-4W.

It should be noted that the partially unconverted B-PES layer at the bottom can serve as mechanical support for the electrode material, which the electrodes prepared in this study are

self-supporting electrodes.

Material characterization

The surface morphology of all samples was observed by fieldemission scanning electron microscopy (FESEM, Hitachi, Japan, JEOL-7500F) operated at 10 kV. The average thickness of the as-prepared products was calculated by the cross-section SEM. The structure of all samples was evaluated on a Philips X′pert diffractometer (Rigaku D/MAX-2500/PC) equipped with Cu K radiation (λ = 1.5418 Å). The 2θ range was setting from 5^0 to 70^0 at scan rate of 0.5 min−1. Transmission electron microscopy (TEM, FEI) images were measured on a JEOL JEM-2100F with an accelerating voltage of 300 kV and the detailed morphology of inside the materials was got. The selected area electron diffraction (SAED) was well gained by HRTEM. X-ray photoelectron spectroscopy (XPS, Thermo Scientific K-Alpha) were utilized to analyze crystal conformation of samples.

Electrochemical measurement

All electrochemical tests were performed at electrochemical workstation (CHI760E, Shanghai Chenhua Device Company, China). In three-electrode system, the as-prepared electrode, platinum sheet, Ag/AgCl and 2 M KOH were chosen as the working, counter, reference electrodes and electrolyte, respectively. Electrochemical measurements including cyclic voltammetry (CV), galvanostatic charge-discharge (GCD), electrochemical impedance spectroscopy (EIS), among them, all EIS tests are conducted under open circuit voltage, the same frequency range (10^{-1} Hz – 10^5 Hz) and the fixed amplitude of 5 mV.

Calculation method

According to the discharge branch in GCD curves, the areal specific capacitance (C_A, mF cm^{-2}) uses electrode quality as base for more applicable evaluation, the equation is as follows:

$$C_A = \frac{I \times \Delta t}{\Delta V \times S} \qquad \text{(Equation S1)}$$

Where I, Δt, ΔV and S are the discharge current (A), the discharge time (s), the

GCD discharge voltage range (V, excluding voltage drop) and area of electrodes (1 cm^2), respectively.

In addition, the areal specific capacitance (C_A, mF cm^{-2}) of ASC devices was calculated with Equation S1.

The areal power density (P_A, mW cm^{-2}) and areal energy density (E_A, μWh cm^{-2}) of the ASC devices were achieved via the Equations S2 and S3:

$$E_A = \frac{C_A \times \Delta V}{7.2} \quad \text{(Equation S2)}$$

$$P_A = \frac{3.6 \times E_A}{\Delta t} \quad \text{(Equation S3)}$$

Here, C_A, ΔV, and Δt represent the areal specific capacity (mF cm^{-2}), operating voltage (V) and discharge time (s) of the ASC devices, respectively.

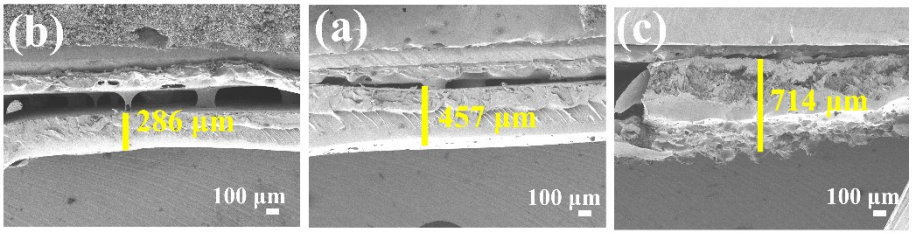

Fig. S1 Cross-sectional SEM images of PES film, BPES film and BS-LIG NPES film

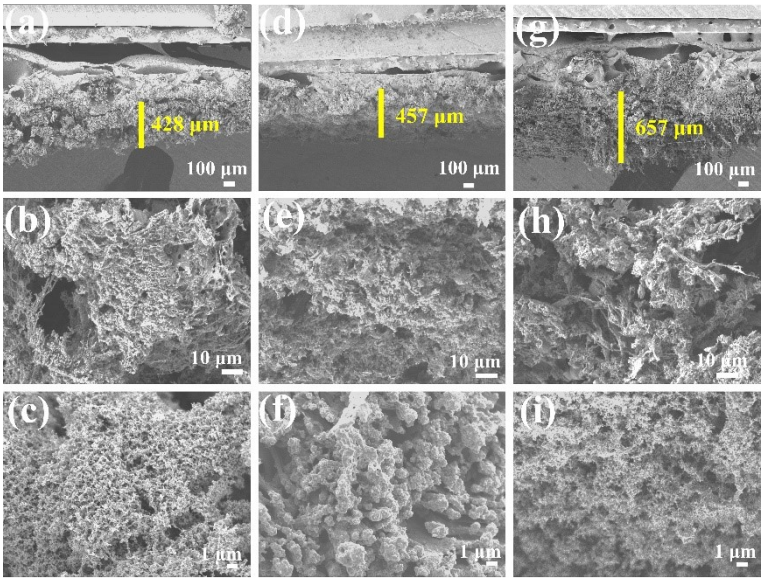

Fig.S2 (a, b) Cross-sectional SEM images of NS-LIG, (c) Top view SEM image of NS-LIG, (d, e) Cross-sectional SEM images of BNS-LIG, (f) Top view SEM image of BNS-LIG, (g, h) Cross-sectional SEM images of (BN)S-LIG, (i) Top-view SEM image of (BN)S-LIG, Laser power is 6 W.

Table S1 The content of different elements in NBS-LIG and BNS-LIG obtained from EDX

	NBS-LIG		BNS-LIG	
	Mass%	Atom%	Mass%	Atom%
C	89.73	90.23	88.46	89.11
S	0.75	0.28	0.35	0.13
O	2.29	1.73	4.11	3.11
B	5.99	6.69	6.02	6.74
N	1.24	1.07	1.06	0.91

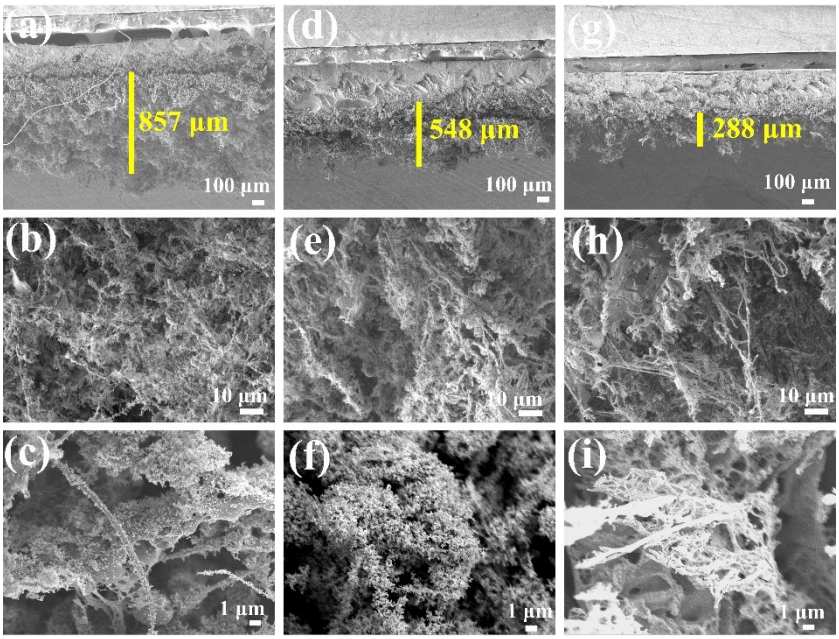

Fig.S3 (a,b) Cross-sectional SEM images of S-LIG-4W, (c) Top-view SEM image of S-LIG-4W(d,e) Cross-sectional SEM images of BS-LIG-4W, (f) Top-view SEM image of BS-LIG-4W

(g,h) Cross-sectional SEM images of NBS-LIG-4W, (i) Top-view SEM image of NBS-LIG-4W

Laser power is 4 W.

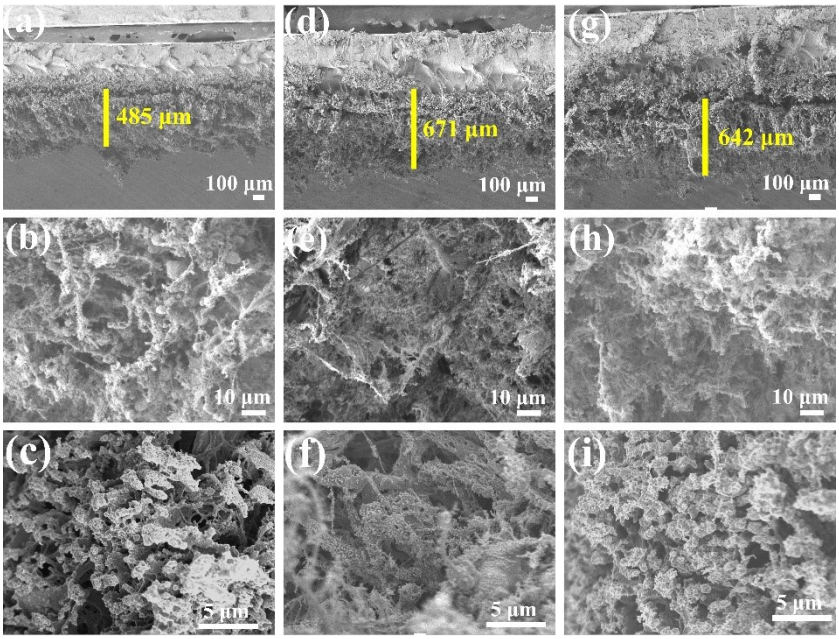

Fig.S4 (a, b) Cross-sectional SEM images of NS-LIG-4W, (c) Top view SEM image of NS-LIG-4W, (d, e) Cross-sectional SEM images of BNS-LIG-4W, (f) Top view SEM image of BNS-LIG-4W, (g, h) Cross-sectional SEM images of (BN)S-LIG-4W, (i) Top-view SEM image of (BN)S-LIG-4W, Laser power is 4W.

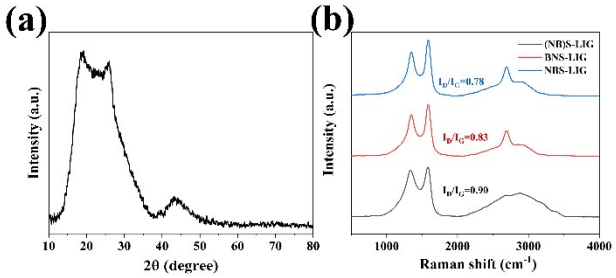

Fig. S5 XRD pattern of NBS-LIG and Raman spectra of (NB)S-LIG, BNS-LIG and NBS-LIG

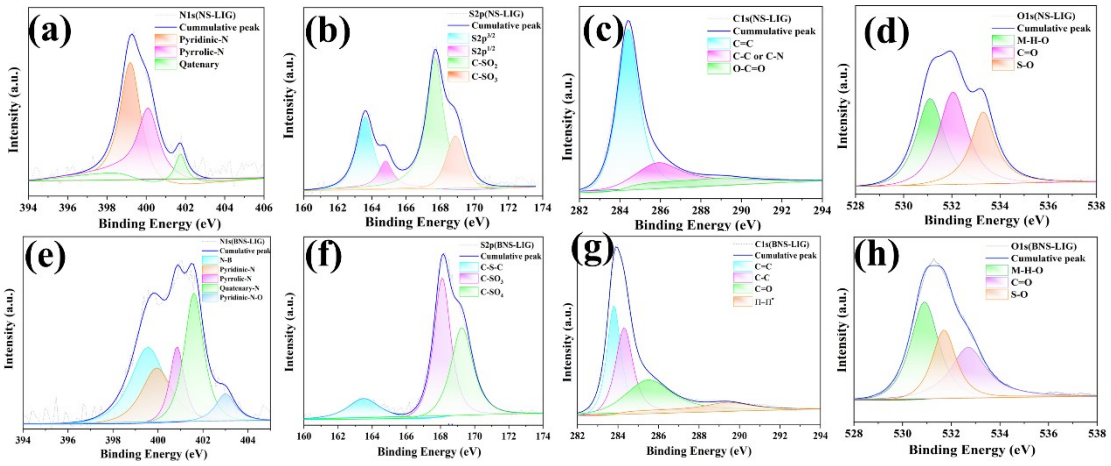

Fig. S6 The high-resolution XPS fitting peaks of B1s (a), S2p (b), C1s (c), O1s (d) spectra of NS-LIG, B1s (e), S2p (f), C1s (g), O1s (h) spectra of BNS-LIG

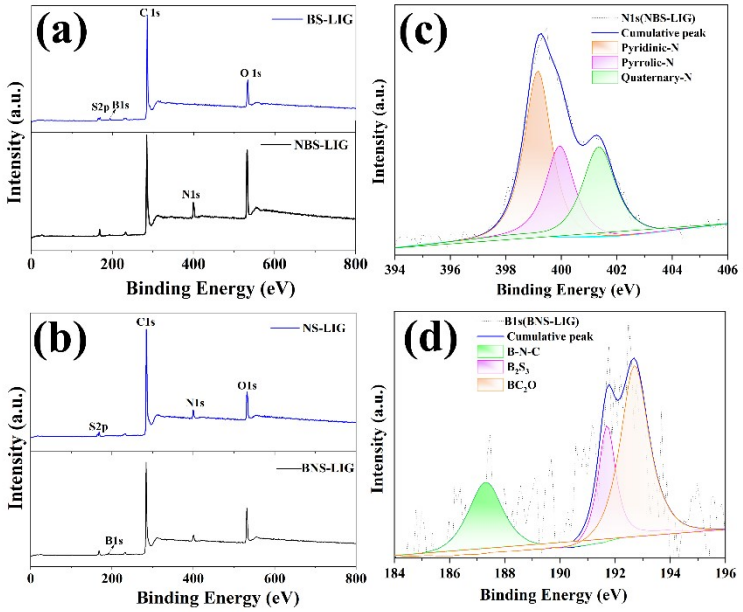

Fig. S7 (a) XPS survey scan spectra of BS-LIG and NBS-LIG, (c) XPS survey scan spectra of NS-LIG and BNS-LIG, High-resolution (b) N 1s spectra of NBS-LIG and (d) B1s spectra of BNS-LIG

Table S2. Elemental composition of carbon, oxygen, nitrogen, and boron elements present in BS-LIG, NBS-LIG, NS-LIG and BNS-LIG

Sample (s)	Carbon (at.%)	Boron (at.%)	Nitrogen (at.%)	Sulfur (at.%)	Oxygen (at.%)
BS-LIG	82.15	4.02	0	2.7	11.13
NBS-LIG	65.29	5.13	7.57	2.84	19.18
NS-LIG	81.59	0	5.03	2.68	10.7
BNS-LIG	74.4	4.29	4.55	2.88	13.87

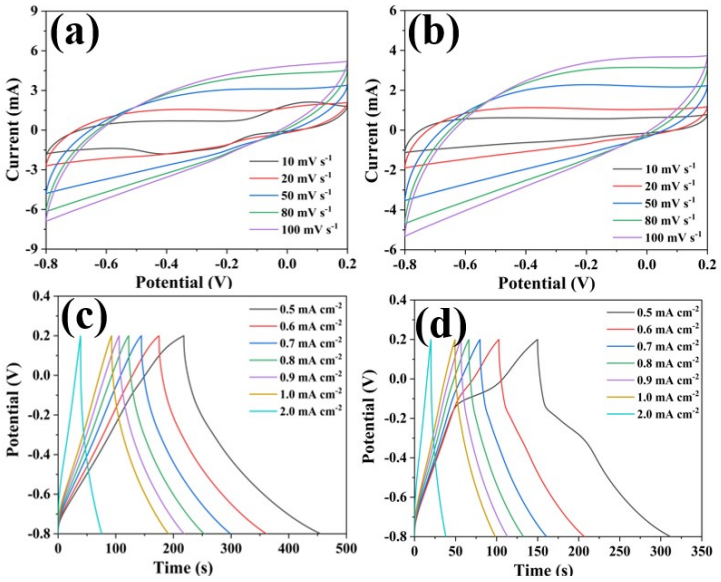

Fig. S8 CV curves of BNS-LIG (a), (NB)S-LIG (b) and GCD curves of BNS-LIG (c), (NB)S-LIG (d) at the laser power of 6 W

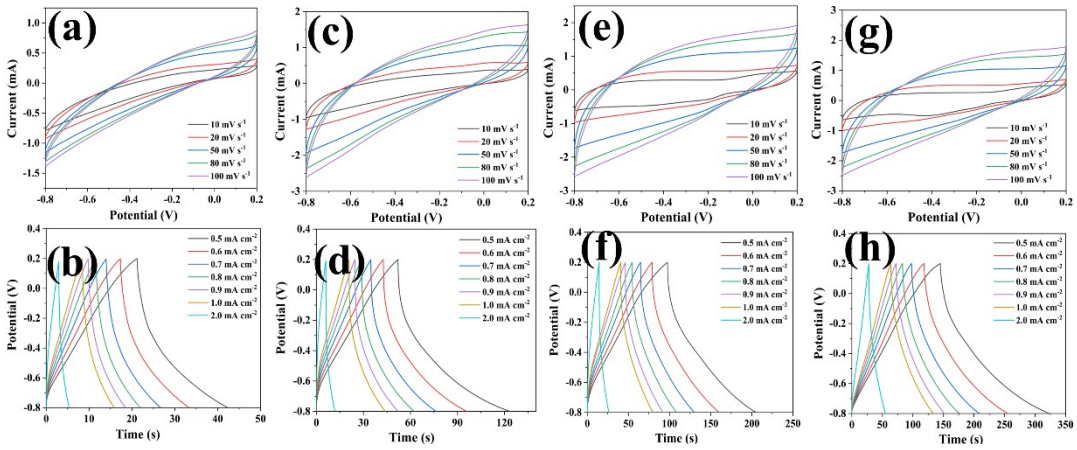

Fig. S9 CV curves of S-LIG-4W (a), (NB)S-LIG-4W (c), BNS-LIG-4W (e), NBS-LIG-4W (g), GCD curves of S-LIG-4W (b), (NB)S-LIG-4W (d), BNS-LIG-4W (f), NBS-LIG-4W (h) at the laser power of 4 W.

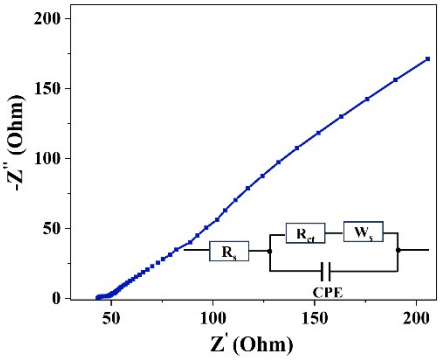

Fig. S10 EIS curves of NBS-LIG SC

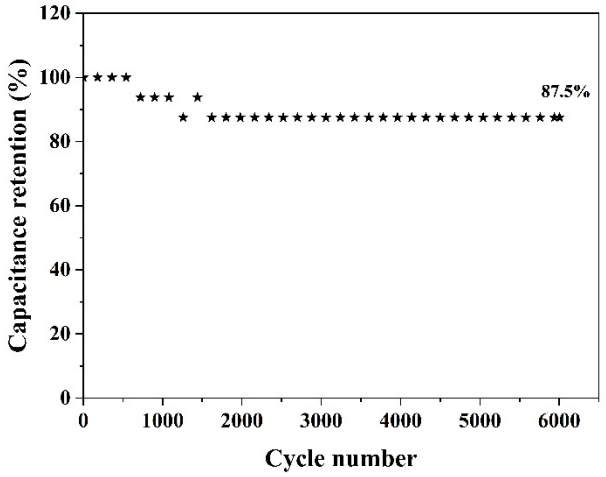

Fig. S11 Cycling stability test of NBS-LIG SC at the current of 1 mA cm^{-2}

Table S3 A comparison of electrochemical performance of NBS-LIG SC fabricated in the present work with some of the previously reported undoped and doped LIG

Electrode material(s)	Electrolyte	C_A (mF cm^{-2})	The minimum current density (mA cm^{-2})	Ref(s).
NBS-LIG-SC	2M KOH	29.1	0.4	This work
N-dLIG-SC	PVA-H_2SO_4	20.8	0.05	[1]
B-LIG	PVA-H_2SO_4	16.5	0.05	[2]
LIAG	PVA-H_3PO_4	32.0	0.05	[3]
LIG	1 M H_2SO_4	~3.9	0.2	[4]
d-LIG	PVA-H_2SO_4	8.0	0.1	[5]
5B-LIG	PVA-H_2SO_4	16.5	0.05	[6]
N-LIG	PVA-H_2SO_4	19.8	0.05	[7]
P-L LIG-P15	PVA-H_2SO_4	22	0.05	[8]
LIG	H_2SO_4	3.9	0.2	[4]
LSG-P24	PVA-H_2SO_4	25.1	0.05	[9]
Ph-ddm LIG	H_2SO_4	22.2	0.2	[10]

References:

[1] R. Nandee, M. Chowdhury, A. Shahid, N. Hossain, M. Rana, *Results in Engineering*, 2022, 15, 100474.

[2] Z. Peng, R. Ye, J.A. Mann, D. Zakhidov, Y. Li, P.R. Smalley, J. Lin, J.M. Tour, *ACS Nano*, 2015, 9(6), 5868-5875.

[3] H. Liu, Y. Xie, J. Liu, K.-s. Moon, L. Lu, Z. Lin, W. Yuan, C. Shen, X. Zang, L. Lin, Y. Tang, C.-P. Wong, *Chem. Eng. J.*, 2020, 393, 124672.
[4] J. Lin, Z. Peng, Y. Liu, F. Ruiz-Zepeda, R. Ye, E.L.G. Samuel, M.J. Yacaman, B.I. Yakobson, J.M. Tour, *Nat. Commun.*, 2014, 5(1), 5714.
[5] J.B. Lee, J. Jang, H. Zhou, Y. Lee, J.B. In, *Energies*, 2020, 13(24), 6567.
[6] Z. Peng, R. Ye, J.A. Mann, D. Zakhidov, Y. Li, P.R. Smalley, J. Lin, J.M. Tour, *ACS Nano*, 2015, 9(6): 5868-5875.
[7] K.Y. Kim, H. Choi, C.V. Tran, J.B. In, *J. Power Sources*, 2019, 441, 227199.
[8] X. Sun, X. Liu, F. Li, *Appl. Surf. Sci.*, 2021, 551, 149438.
[9] W. Zhang, Y. Lei, F. Ming, Q. Jiang, P.M.F.J. Costa, H.N. Alshareef, *Adv. Energy Mater.*, 2018, 8, 1801840.
[10] L. Cao, S. Zhu, B. Pan, X. Dai, W. Zhao, Y. Liu, W. Xie, Y. Kuang, X. Liu, *Carbon*, 2020, 163: 85-94.